FUSE 900–1200Å Spectroscopy of AM Her[1]

J.B. Hutchings

Herzberg Insitute of Astrophysics, National Research Council of Canada,

Victoria, B.C. V8X 4M6, Canada

john.hutchings@nrc.ca

A.W. Fullerton

Dept. of Physics and Astronomy, University of Victoria

P.O. Box 3055, Victoria, B.C. V8W 3P6, Canada

Dept. of Physics and Astronomy, Johns Hopkins University

3400 N. Charles St., Baltimore, MD 21286

awf@pha.jhu.edu

A.P. Cowley[1], P.C. Schmidtke[1]

Dept. of Physics & Astronomy, Arizona State University, Tempe, AZ, 85287-1504

anne.cowley@asu.edu; paul.schmidtke@asu.edu

Received _____; accepted _____

[1]Based on observations made with the NASA-CNES-CSA Far Ultraviolet Spectroscopic Explorer. FUSE is operated for NASA by the Johns Hopkins University under NASA contract NAS5-3298

ABSTRACT

Spectra of the magnetic white dwarf binary AM Her were obtained with the Far Ultraviolet Spectroscopic Explorer (FUSE) during three consecutive spacecraft orbits. These observations were split into 19 spectra of about 5 min duration (0.025P binary phase) partially covering the binary orbit. We report the phase-related changes in the far ultraviolet continuum light curve and the emission lines, noting particularly the behavior of O VI. We discuss the fluxes and velocities of the narrow and broad O VI emissions. We find the FUV light curve has maximum amplitude at ∼1000Å, although at shorter wavelengths the continuum may be strongly affected by overlapping Lyman lines. Weak, narrow Lyman absorption lines are present. Their velocities don't appear to vary over the observed orbital phases, and their mean value is consistent with the systemic velocity.

Subject headings: ultraviolet: stars – cataclysmic variables – binaries: close – stars: individual: AM Her

1. Introduction

AM Her, originally classified as an irregular variable and associated with the X-ray source 3U 1809+50, was discovered in 1976 to be a short period binary related to the cataclysmic variables (CVs) (Szkody & Brownlee 1997, Cowley & Crampton 1977, Priedhorsky 1977). Through its 3.1-hr orbital period, AM Her's brightness varies continuously, with short-term flickering superimposed on an orbital light curve with a range of $\Delta V \sim 0.7$ mag. Independently, Tapia (1977) found the same orbital period from polarization variations indicating that the white dwarf in the system has a very strong magnetic field ($B \sim 2 \times 10^8$ gauss) and rotates synchronously with the orbit. The magnetic field constrains the mass lost from the secondary star to flow along a stream directly onto the white dwarf rather than into an accretion disk as in the non-magnetic CVs.

The optical spectrum shows strong emission lines of H, He I, and He II, along with weaker lines of other ions such as N III, C III, C II, and Ca II, all showing large velocity variations. The strong lines show both broad and narrow components which clearly arise in different regions since their phasing and velocity amplitudes differ considerably (e.g. Crampton & Cowley 1977, Crosa et al. 1981, and many more recent studies). TiO bands from the M4 V secondary star are detected when the system is in its faint ("low") state (e.g. Young, Schneider, & Shectman 1981).

Even early observations showed light curves and times of minima in V, U, and X-ray bands to be quite different (e.g. see Fig. 6 of Crampton & Cowley, 1977). Subsequent observations in other wavelengths have revealed additional complex patterns of orbital behavior, much of which can be interpreted as a result of the strong magnetic field. Gänsicke et al. (2001) attribute the V-band light curve to cyclotron emission arising near the accreting magnetic pole, the small B-band variation to the accretion stream, and the hard X-ray variation to the changing view of the hot plasma at the shock where

stream impacts the white dwarf. Because times of minima depend on the wavelength of observation, there is some uncertainty about what ephemeris to use. In this paper we adopt the well-determined period given by Heise & Verbunt (1988) and a phase based on our time of FUV minimum light. In other published work often the adopted T_0 is the time of minimum V light which corresponds approximately to the superior conjunction of the white dwarf (e.g. Gänsicke et al. 1998, Southwell et al. 1995).

Although AM Her usually remains in its 'high' state (V ∼13 mag), from time to time it drops into a 'low' state (V below 15 mag) which may last weeks or months (e.g. Mattei 1980). A plot of the long-term light curve from 1977 to 1998 is shown in Fig. 1 of Hessman, Gänsicke, & Mattei (2000), which nicely illustrates the high and low states of AM Her. Although the system underwent a rather prolonged low state a few years ago (e.g. de Martino et al. 1998), the FUSE data described in the present paper were obtained during a normal 'high' state, with magnitude close to $V \sim 13.3$, as is shown by the on-line AAVSO database.

AM Her has become the proptotype of the class of magnetic CVs, commonly called "polars", in which the rotation period of the white dwarf is locked to the orbital period. An excellent summary of the properties of these systems is given by Warner (1995).

2. FUSE Observations

Observations of AM Her were made with the Far Ultraviolet Spectroscopic Explorer (FUSE) on 2000, June 12-13 using the large science aperture and recording the data in time-tag mode. The observations covered three FUSE orbits, and the archival processing (Calfuse 1.6.9) produced three spectra - one for each FUSE orbital window. We also re-extracted the spectra with Calfuse 1.9.9, with the time-tagged data split into 19 individual

spectra of duration 0.0033 days each (4.75 min, or 0.025P in binary orbital phase). Because of earth occultations, there are gaps in the phase coverage so that only about half the orbit is well sampled. This includes phases Φ_{UVmin}=0.28-0.52 and 0.84-0.97, using an ephemeris based on the period given by Heise & Verbunt (1988) and T_0 corresponding to the time of minimum far-ultraviolet light (as given in §4). However, the observed phases do cover two main portions of the orbit, about 180° apart, with some phase overlap. The spectra have sufficient signal and time resolution to obtain phase-related information.

3. FUSE Spectrum of AM Her

Figure 1 shows two spectra obtained from the entire second and third FUSE orbits. These spectra cover the phases near minimum and maximum FUV light. Stellar emission features which are present include O VI 1032, 1038Å, He II 1085 Å, N III 992Å, C III 977, 1175Å, and S IV 1073Å. These lines are labelled in Fig. 1, and their rest wavelengths are marked. Note the continuum differences and the changes in the emission line structure between the two spectra.

Measurements of these lines are given in Table 1. The HJDs in the table have been converted from the MJDs provided in the FUSE data header, and the heliocentric time correction has been added. Heliocentric velocity corrections are included in the standard FUSE reductions. Most of these lines were previously observed with *ORFEUS II* and Hopkins Ultraviolet Telescope (HUT), but with lower spectral resolution (Mauche & Raymond 1998, Greeley et al. 1999).

The strong narrow emission lines in the summed spectra are mainly airglow, except for the narrow component in the O VI lines. O VI shows both a broad and a narrow emission component, similar to the structure seen for the strongest lines in the optical and ultraviolet

regions. There is also broad emission from the stronger Lyman lines. Gänsicke et al. (1998) point out that in the UV only the highest excitation lines (N V and Si IV) show this broad plus narrow line structure, while the lower ionization features of C II, C III, Si II, and Si III show only the broad component. In the FUV we similarly find that the C III lines (and probably the Si IV lines, which are weaker) have only the broad emission line, although the profiles change significantly with binary phase.

Narrow Lyman absorption lines are seen below 950Å, especially noticeable in the spectrum at maximum FUV light. These were not observed in the *ORFEUS II* spectra, probably because of their lower resolution. There is only weak evidence for any H_2 absorption, in strong contrast to the supersoft X-ray binary QR And in which Hutchings et al. (2001) found probable circumbinary as well as interstellar H_2 absorption.

Airglow emissions lie in the middle of the N III 992Å and He II 1085Å emission lines, making it difficult to make clean measurements of these features. While there are some airglow lines near the O VI lines, we can make use of the doublet to isolate these fairly well. The strong C III 1175Å line is free of airglow and shows very different profile changes from O VI, as described in §5 below.

4. FUV Continuum Changes and Adopted Phases

There are continuum changes across the whole FUSE range. We have defined a FUV phase, using the period of Heise & Verbunt (1988) and the time of minimum FUV light from our FUSE data. The continuum light curve used for our ephemeris is based on the total signal from the LiF1a channel, after removal of the strong airglow emissions. This channel has the best guiding and signal levels in the FUSE data. As discussed below, there are differences within the FUSE band, so we also measured the continuum over several ranges

Table 1. Spectroscopic Data and Measurements

HJD 2451700+	FUV[1] Phase	Flux 980–1090Å (erg/cm^2/sec/Å)	O VI peak (km s^{-1})	O VI broad (km s^{-1})	C III broad (km s^{-1})
8.4956	0.281	2.25×10^{-13}	−27, −36	214, —	300
8.4989	0.306	2.62×10^{-13}	−33, −18	69, 63	430
8.5023	0.333	2.94×10^{-13}	−38, −47	159, −27	425
8.5056	0.358	3.09×10^{-13}	−41, −53	252, 97	305
8.5089	0.384	3.21×10^{-13}	−44, −47	66, 251	610
8.5122	0.410	3.03×10^{-13}	−47, −44	267, 245	355
8.5155	0.435	3.18×10^{-13}	−53, −44	110, 126	530
8.5676	0.839	1.55×10^{-13}	66, 57	−247, −189	−180
8.5709	0.865	1.45×10^{-13}	95, 71	−294, −348	−230
8.5742	0.890	1.31×10^{-13}	69, 66	−172, −333	−225
8.5775	0.916	1.06×10^{-13}	66, 83	−201, −119	−280
8.5808	0.942	1.03×10^{-13}	89, 83	−178, −134	−260
8.5841	0.967	0.94×10^{-13}	81, 80	−152, −206	−255
8.6385	0.389	3.04×10^{-13}	−44, −50	113, 216	150
8.6418	0.415	3.00×10^{-13}	−53, −41	113, 57	250
8.6451	0.440	3.20×10^{-13}	−41, −50	101, 112	100
8.6484	0.466	3.50×10^{-13}	−35, −38	127, —	200
8.6517	0.492	3.27×10^{-13}	−33, −10	211, 222	250
8.6550	0.517	3.38×10^{-13}	−33, −33	142, 199	300

[1]Ephemeris: $T_0(FUVmin)$ = HJD 2451708.4594 + 0.128927041E; see text

of wavelengths (see Figure 2, lower panel). Although all the continuum flux datasets are well fit by a sine curve, we have used the fit for 980-1090Å to define the time of minimum FUV flux and hence our zero phase (Φ_{FUVmin}=0.0). Table 2 shows the parameters of the fits for various wavelength ranges. We adopt:

$$\Phi_{FUVmin} = 0 = \text{HJD } 2451708.4594(11) + 0.128927041(5)\text{E}$$

Comparing this to other phase conventions used in the literature, we find $\Phi_{mag} = \Phi_{FUV}$ + 0.11 (based on the ephemeris given by Heise & Verbunt 1988). Similarly orbital phases, where zero phase is the superior conjunction of the white dwarf, are $\Phi_{orb} = \Phi_{mag} + 0.37 = \Phi_{FUV} + 0.48$ (using information from Southwell et al. 1995 and Gänsicke et al. 1998). The problem with these alternative zero points is that they are defined by older data, so here we prefer to use only our FUV data to avoid possible error accumulation over many years.

The phasing for our FUV light curve is very similar to that observed in other ultraviolet and far-ultraviolet studies. Using IUE data, Gänsicke, Beuermann, & de Martino (1995) found the flux at λ1460 brightest at $\Phi_{mag} \sim 0.6$ and faintest at $\Phi_{mag} \sim$0.1 (see their Fig. 5). From HST data, Gänsicke et al. (1998) observed similar phasing for three different wavelength regions between 1150Å and 1427Å, with the amplitude increasing towards shorter wavelengths (see their Fig. 3). Greeley et al. (1999), using HUT data, found the peak brightness at the Lyman limit occurred at $\Phi_{mag} \sim 0.6$, and Mauche & Raymond (1998) found the flux at 1010Å also peaked at magnetic phase ∼0.6. Formally, our peak occurs at $\Phi_{mag} = 0.61$. Thus, all of these independent data sets are consistent in the phasing of the UV and FUV light curves.

However, in our FUSE data the continuum shows a deeper minimum over the wavelength range 950-1050Å than outside that range, with the deepest minimum occuring at ∼1000Å. There the total flux range is a factor six, compared with three or less elsewhere. This deep minimum occurs over several FUSE detector channels, and thus is unlikely to

be a detector, data processing, or tracking artifact. Figure 2 shows our light curves from the 1000Å region and a longer wavelength region (1090-1180Å). Similarly, Gänsicke et al (1998) found a trend for the amplitude of the modulation to be largest at their shortest wavelength region which was centered on 1158Å, but their HST observations did not go into the shorter wavelength region covered by the FUSE data.

Mauche & Raymond (1998) reported a flux range of a factor ∼3.3 at 1010Å from their *ORFEUS II* data, and they did not note any differences at other wavelengths. They fit the continuum with a two-temperature model, but there are deviations from it at wavelengths shorter and longer than 1000Å. Hence, the effect of a larger variation at ∼1000Å may be present in their data as well, or there may be some change in the FUV flux between their observations and ours. They have modeled the light curves with cyclotron components in the visible region and with a localized hotspot on the white dwarf surface in the FUV.

Our wavelength-dependent light curve is not seen in the broad-line wings when we take ratios of the two spectra. This is demonstrated in Figure 3, where the broad regions around the strong emission lines show the shallower minima seen in the continuum below 950Å and above 1050Å. This suggests that there are very wide wings associated with the strong emissions which fully overlap in the higher Lyman lines. These features are visible in the ratio of any two of the three FUSE orbits, all of which have different binary phase coverage, but it is strongest in the ratio shown in Figure 3, covering the largest continuum changes. If the ratio in the shortest wavelengths is affected by overlapping Lyman lines, it is possible that the real continuum variation remains high at all wavelengths below about 1000Å. Such a scenario is indicated schematically in Fig. 3 by the dotted line. This line is not calculated, but merely drawn in to show a real continuum that would be feasible with broad-line blanketing, and compatible with the white dwarf hot-spot model.

5. Emission Line Measurements and Changes

The O VI lines are higher ionization lines than any emission observed in the HST or optical ranges, and thus they are potentially of unique interest. They have been observed previously in two visits by *ORFEUS* (in 1993 and 1996). The 1996 data are superior and were taken when AM Her was in a high state (see Mauche & Raymond 1998). The behavior of the O VI lines is similar to the He II line at 4686Å in having sharp and broad components with very different velocity amplitudes and phasing (see e.g. Cowley and Crampton 1977).

Line velocities were measured by fitting a parabola to the entire feature, and also by taking the flux centroid of the emission line. Values given are the mean of the separate measures. The broad component of the O VI doublet shows a velocity semi-amplitude K$\sim$190 km s^{-1} with the minimum velocity at $\Phi_{FUV} \sim 0.9$ (or approximately $\Phi_{mag} \sim 0.0$), whereas the narrow component shows K of only 62 km s^{-1} with phasing about half a cycle later. These values can be directly compared to the measurements made by Mauche & Raymond who had fewer spectra but more evenly distributed around the orbit. Their amplitudes for the broad and narrow components of O VI were K=412 and 57 km s^{-1}, respectively, with phasing very similar to what we observe after taking into account the difference between FUV and magnetic phases.

Additionally, there is a broad component of Lβ, easily seen on either side of the airglow emission. While blended with the airglow emission, it appears to have a similar line profile and to move with the broad O VI lines (see Fig. 4). This broad emission component is also present in the other strong Lyman lines where it is too weak to measure. Figure 2 includes our flux and velocity measurements of Lβ. The broad Lβ line shows greater fractional change than the broad O VI, so that their ratio changes markedly at phases Φ_{FUV}=0.4 to 0.5.

We also measured the flux and velocity of the C III emission line at 1175Å. This line

is broad and has no narrow component significantly different from the noise level. We have also summed the spectra in groups of three to increase the signal-to-noise in the line profile. Its overall profile changes strongly, as shown in Figure 5. Using the C III velocities from all 19 spectra (to retain the maximum phase resolution), we obtained the sine-curve fit given in Table 2. Both the semi-amplitude (K=311 km s^{-1}) and the mean value (+50 km s^{-1}) are significantly different from the fit found for the broad O VI lines. Gänsicke et al. found C III 1176Å to have a semi-amplitude of 540 km s^{-1} with the minimum velocity occurring about 0.1P later than we observe. However, their HST data had more complete phase coverage, so these two C III lines probably behave similarly.

The other emission lines were weaker and contaminated with airglow emissions, so we were not able to measure them. However, Fig. 3 suggests the presence of other possible emission features if the dips are all caused by line broad line emission that has a lower flux variation than the continuum. This idea is reinforced by the fact that these wavelengths correspond to those of possible emission lines. Along the bottom of this figure we have marked the positions of the identified lines we measured, as well as the stronger S IV line positions - all of which lie at dips in the ratio plot. Thus, we conclude that several weak S IV emission features may be present that do not show up clearly in either the individual or summed spectra.

While the phasing of FUV continuum are in good agreement with those of Mauche & Raymond and with the UV data of Gänsicke et al., the velocity amplitudes of the broad lines differs, as described above. Our amplitudes are less well-defined because of our more limited phase coverage, but they do appear to cover the velocity extremes fairly well.

Table 2. Sine Curve Fits to Measurements

Quantity	Minimum HJD 2451700+	$\Delta\phi$ phase[a]	Semi-amplitude K	Mean Value	Mean Error
Flux			mag	erg/cm^2/sec/Å	mag
980–1090Å	8.4594±0.0011	(0.0)	0.65±0.05	2.17×10^{-12}	0.05
994–1020Å	8.4585±0.0011	0.993±0.009	1.20±0.05	1.84×10^{-13}	0.08
1090–1180Å	8.4619±0.0011	0.019±0.009	0.61±0.05	2.17×10^{-13}	0.05
Velocity			km s^{-1}	km s^{-1}	km s^{-1}
O VI broad	8.4479±0.0041	0.910±0.03	190±15	−30±14	79
O VI peak	8.3828±0.0014	0.406±0.01	62±2	16±2	9
C III broad	8.4416±0.005	0.862±0.04	311±38	50±31	125

[a]Phase of minimum flux or velocity, with respect to FUV ephemeris

6. Absorption Lines

As noted earlier, H_2 absorption is weak, indicating there is little H_2 along the line of sight. In the supersoft binary system QR And where H_2 was particularly strong, we presented evidence that this absorption was at least partially due to circumbinary material. By comparison, this suggests that little cool gas is leaving the AM Her system. However, we do see a clear set of narrow H absorption lines (see Figure 1). Within the precision of the FUSE wavelength scale at the shortest wavelengths, these H absorptions all show the same velocity and do not change with time. Their mean velocity is -36 ± 8 km s^{-1}, which can be compared to the systemic velocity of -19 km s^{-1} (Young, Schneider, & Shectman 1981). We note however, that our Calfuse 1.9.9 extractions gave different results in the region than the version 1.6.9 pipeline data. We regard ours as better as a) the version 1.6.9 radial velocities range systematically with wavelength while the later version 1.9.9 values do not. The FUSE wavelength scale precision is not well established at the shortward limit, but it is possible that there is a systematic velocity error of order $\sim$20 km s^{-1}.

The Lyman absorption lines between 918 and 950Å were measured for equivalent width. Noting again a difference between our extractions and the pipeline, we find the absorptions have a mean EW of 0.26 ± 0.04Å. There is no significant change with binary phase. Thus, the absorption appears to arise outside the system, and may be normal interstellar gas.

There are several weak to moderate absorption features seen in all spectra in the wavelength range 1036 to 1041Å, where we have good signal and are interested in contamination of the O VI emission. We identify the strongest as the C II doublet at 1036.3, 1037.0Å. Other weak absorptions match the H_2 spectrum at the same velocity (close to zero, subject to the FUSE wavelength scale uncertainty), and also O I. We do not see any changes in these absorptions with binary phase. They are weak enough that they do not affect the O VI line measures significantly.

7. Summary

A general model of the system has been discussed and developed by a number of authors (e.g. Gänsicke et al. 1998 and Mauche & Raymond 1998 are recent examples). There is mass transfer along magnetic field lines within the system, principally on to one pole of the white dwarf, at least in the system high state. This pole is hot and causes the X-ray and UV flux variations as the system rotates. The optical-NIR light changes are caused by a combination of the temperature gradients on both the donor star and the white dwarf. The broad emission lines arise along the path of the gas stream, while the narrow emission lines appear to be located near the cusp of the donor star's Roche lobe. The FUSE data are consistent with this picture, while providing some new details and aspects of the complex system. Our principal results are as follows.

1. The broad O VI emission lines have the same phasing as the other broad emissions, but appear to have a different velocity amplitude from that seen in 1996 in the ORFEUS data. Changes in other broad-line amplitudes have been noted (e.g. by Crosa et al. 1981 for He II 4686Å), and presumably indicate variations in the gas stream ionisation and kinematics, as the mass transfer rate varies.

2. The narrow O VI emission lines also behave much like the other narrow emissions. Our data agree with the ORFEUS results in velocity, but the higher FUSE resolution gives a very different separation of flux between the broad and narrow components. While we do not cover the entire orbit, we find the narrow line to have less that 1/4 the broad line flux at all times and that the narrow line is very weak at FUV light minimum.

The velocities of the narrow lines seem more stable over the history of various investigations and support the standard interpretation that they arise at the Roche lobe cusp. The range of ionization seen (from Ca II to O VI) is very large, and it is clear that some mechanisms other than photoionization are involved. If we examine the velocity

amplitudes for all the lines, there is a trend with ionization potential running from values near 100 km s^{-1} for Ca II and H I to about 60 km s^{-1} for O VI and N V. He I, C II, He II, Si IV, N III are part of the intermediate sequence. As proposed by Gänsicke et al., this suggests an ionization gradient moving away from the Roche lobe cusp towards the system center of mass.

3. The FUV light curve shows strong changes over the FUSE wavelength range. This is compatible with the model of a hot spot on the white dwarf if a significant part of the FUV flux arises as broad line emission from all the lines detected and where the higher Lyman lines overlap each other.

4. We find sharp H I Lyman absorptions with a constant radial velocity of -36 km s^{-1}. Weak H_2 absorption appears to be present, which does not change with binary phase, and has the same velocity as other interstellar absorptions. AM Her's H_2 absorption is much weaker than that in the X-ray binary QR And, which is at a similar distance from us.

The authors acknowledge use of the AAVSO web site and thank the many variable star observers for their contributions to this dataset. APC also acknowledges her support from NASA for this work.

REFERENCES

Cowley, A.P. & Crampton, D. 1977, ApJ, 212, L121

Crampton, D. & Cowley, A.P. 1977, PASP, 89, 374

Crosa, L., Szkody, P., Stokes, G., Swank, J., & Wallerstein, G. 1981, ApJ, 247, 984

de Martino, D., et al. 1998, A&A, 333, L31

Gänsicke, B.T., Beuermann, K., & de Martino, D. 1995, A&A, 303, 127

Gänsicke, B.T., Fischer, A., Silvotti, R., & di Martino, D. 2001, A&A, 372, 557

Gänsicke, B.T., Hoard, D.W., Beuermann, K., Sion, E.M., & Szkody, P. 1998, A&A, 338, 933

Greeley, B.W., Blair, W.P., Long, K.S., & Raymond, J.C. 1999, ApJ, 513, 419

Heise, J. & Verbunt, F., 1988, A&A, 112

Hessman, F.V., Gänsicke, B.T., & Mattei, J.A. 2000, A&A, 361, 952

Hutchings, J.B., Crampton, D., Cowley, A.P., & Schmidtke,

P.C. 2001, AJ, 122, 1572

Mattei, J. 1980, IAU Circ. 3490

Mauche, C.W. & Raymond, J.C. 1998, ApJ, 505, 869

Priedhorsky, W.C. 1977, ApJ, 212, L117

Southwell, K.A., Still, M.D., Smith, R.C., & Martin, J.S.

1995, A&A, 302, 90

Szkody, P. & Brownlee, D.E. 1977, ApJ, 212, L113

Tapia, S. 1977, ApJ, 212, L125

Young, P., Schneider, D.P. & Shectman, S.A. 1981, ApJ, 245, 1043

Warner, B. 1995, Cataclysmic Variable Stars, Cambridge Univ. Press

Fig. 1.— Two AM Her spectra summed from full FUSE orbits (2 and 3), covering FUV phases near maximum and minimum light. The dashed lines show the zero values for the upper spectra. The strong emission lines are marked and identified. The strong narrow emissions (with the exception of O VI) are airglow. Note the broad emission profile changes and the narrow Lyman absorptions.

Fig. 2.— Measurements from 19 equal-exposure FUSE spectra plotted on FUV phases (see text for conversion to binary or magnetic phases). In the valocity panels the open circles are the broad O VI values, the dots the O VI peaks, the asterisks the C III, and the encircled crosses are Lβ. Phase zero is the minimum FUV light from a sine fit to the LiF1a channel data. Note the deeper minimum at $\sim$1000Å than at longer and shorter wavelengths. Other panels show radial velocities from emission-line centroids and total flux in emission-line features.

Fig. 3.— Ratio of FUSE orbit spectra taken near maximum and minimum FUV light (as shown in Fig. 1), after airglow removal and heavy smoothing. Note the strong increase in continuum ratio below 1050Å and the lower amplitude seen in broad 'wings' around the emission lines. The tickmarks show the positions of emission lines, including weak S IV features. It is possible the ratio is low below 960Å because of overlapping Lyman series 'wings'. If so, then the real continuum variation may remain high at all wavelengths below about 1000Å. The dotted line indicates such a possible interpretation, as discussed in the text.

Fig. 4.— The full sequence of O VI and Lβ emissions (with airglow removed). The spectra are smoothed to reduce noise but that has broadened the narrow emissions. Plots are offset by 5×10^{-13} erg cm^{-2} sec^{-1} Å^{-1} in flux. See Table 1 for the FUV phases for each spectrum.

Fig. 5.— Variations in the C III 1175Å line. Three or four spectra have been combined in each plot to show the changes more clearly. Continua, interpolated from adjoining parts of the spectrum, are dotted in. The vertical bars show the velocity centroids of the emission lines. Plots are offset in flux by 2×10^{-13} erg cm^{-2} sec^{-1}, and their mean FUV phases are given. Figure 2 plots measurements from these profiles.

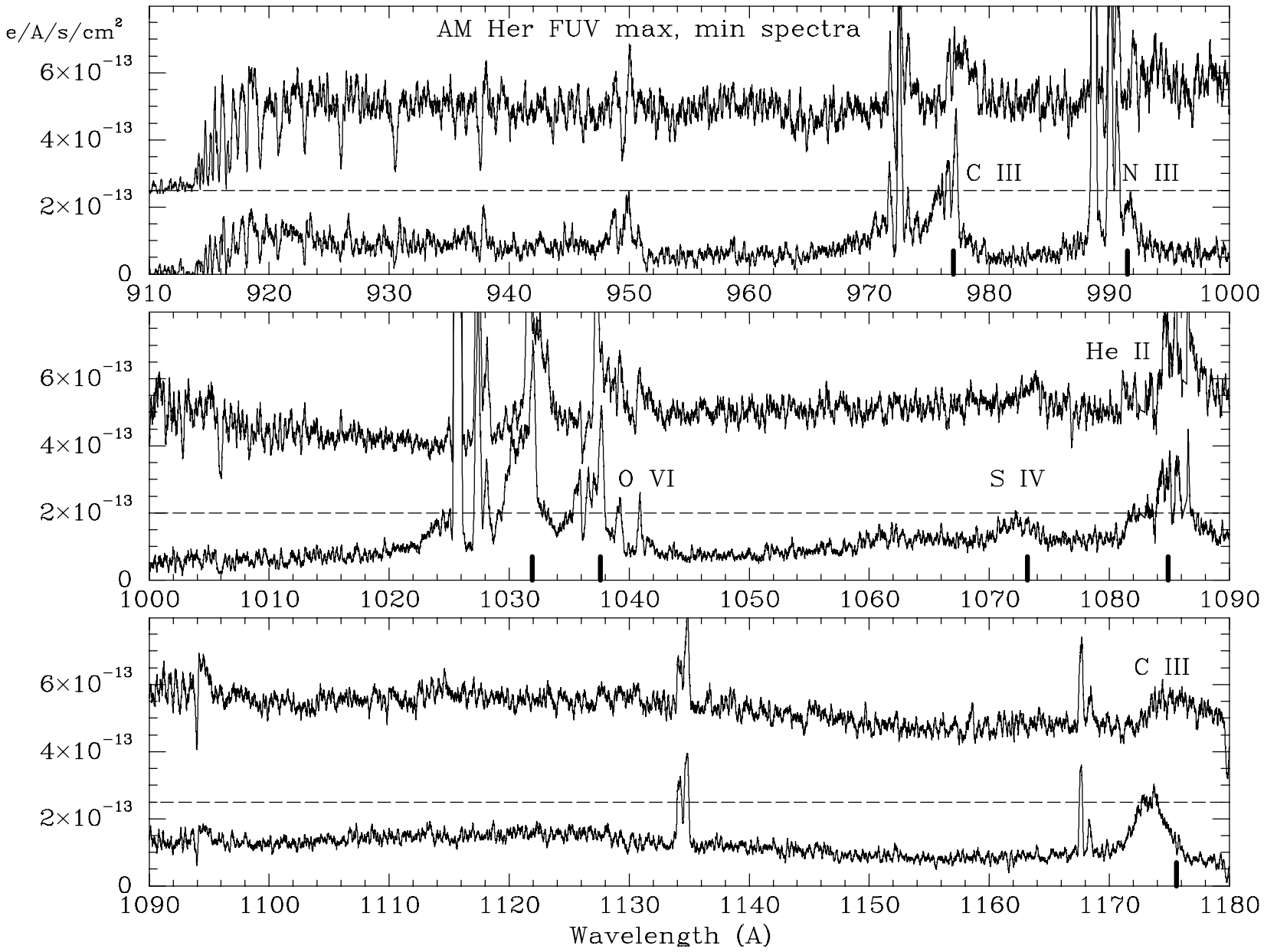
AM Her FUV max, min spectra
e/A/s/cm²
6×10⁻¹³
4×10⁻¹³
2×10⁻¹³
0
C III
N III
He II
O VI
S IV
C III
910
920
930
940
950
960
970
980
990
1000
1010
1020
1030
1040
1050
1060
1070
1080
1090
1100
1110
1120
1130
1140
1150
1160
1170
1180
Wavelength (A)

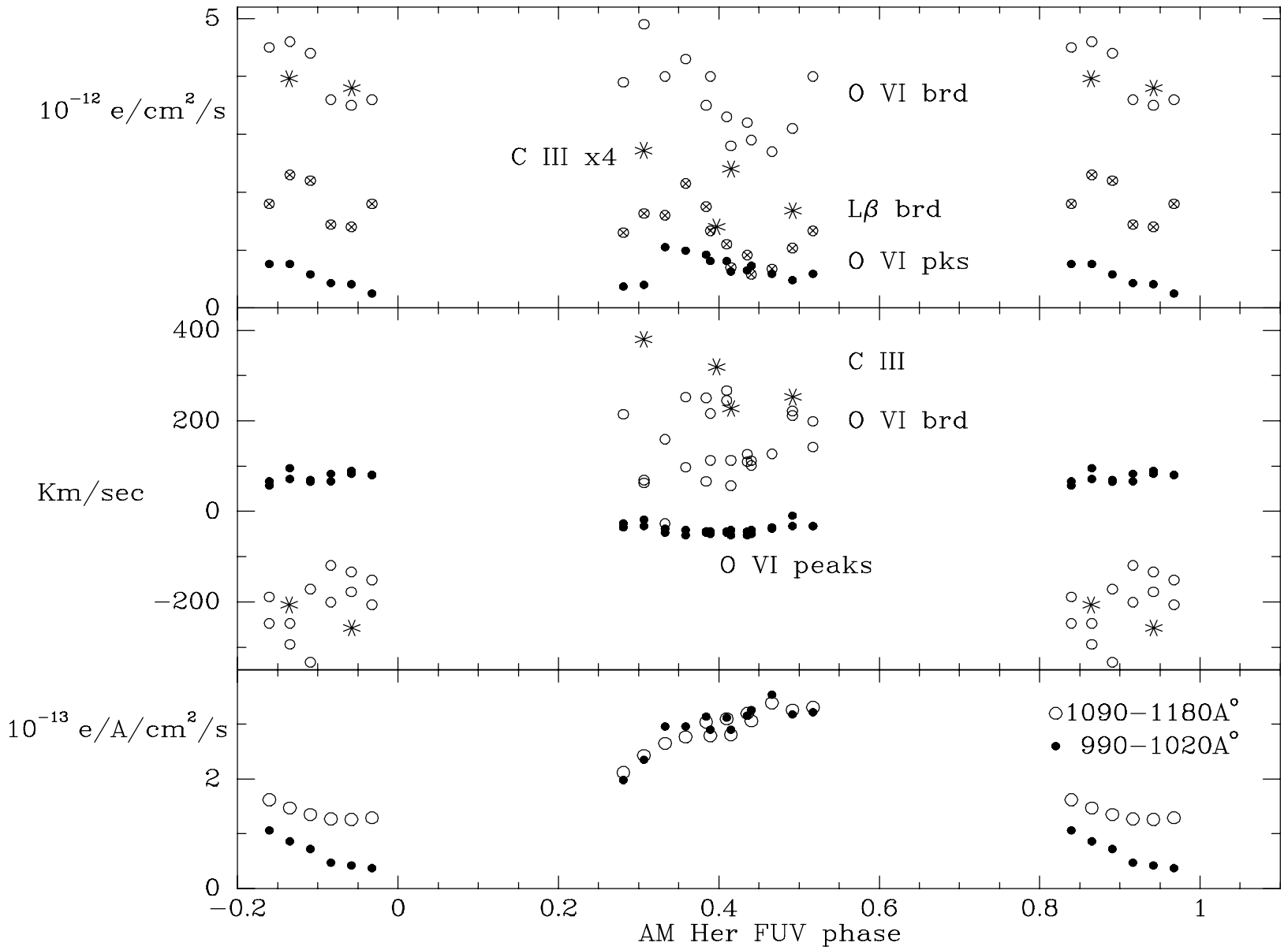
5
10^{-12} e/cm^2/s
0
O VI brd
C III x4
Lβ brd
O VI pks
400
200
Km/sec
0
−200
C III
O VI brd
O VI peaks
10^{-13} e/A/cm^2/s
2
0
1090−1180A°
990−1020A°
−0.2
0
0.2
0.4
0.6
0.8
1
AM Her FUV phase

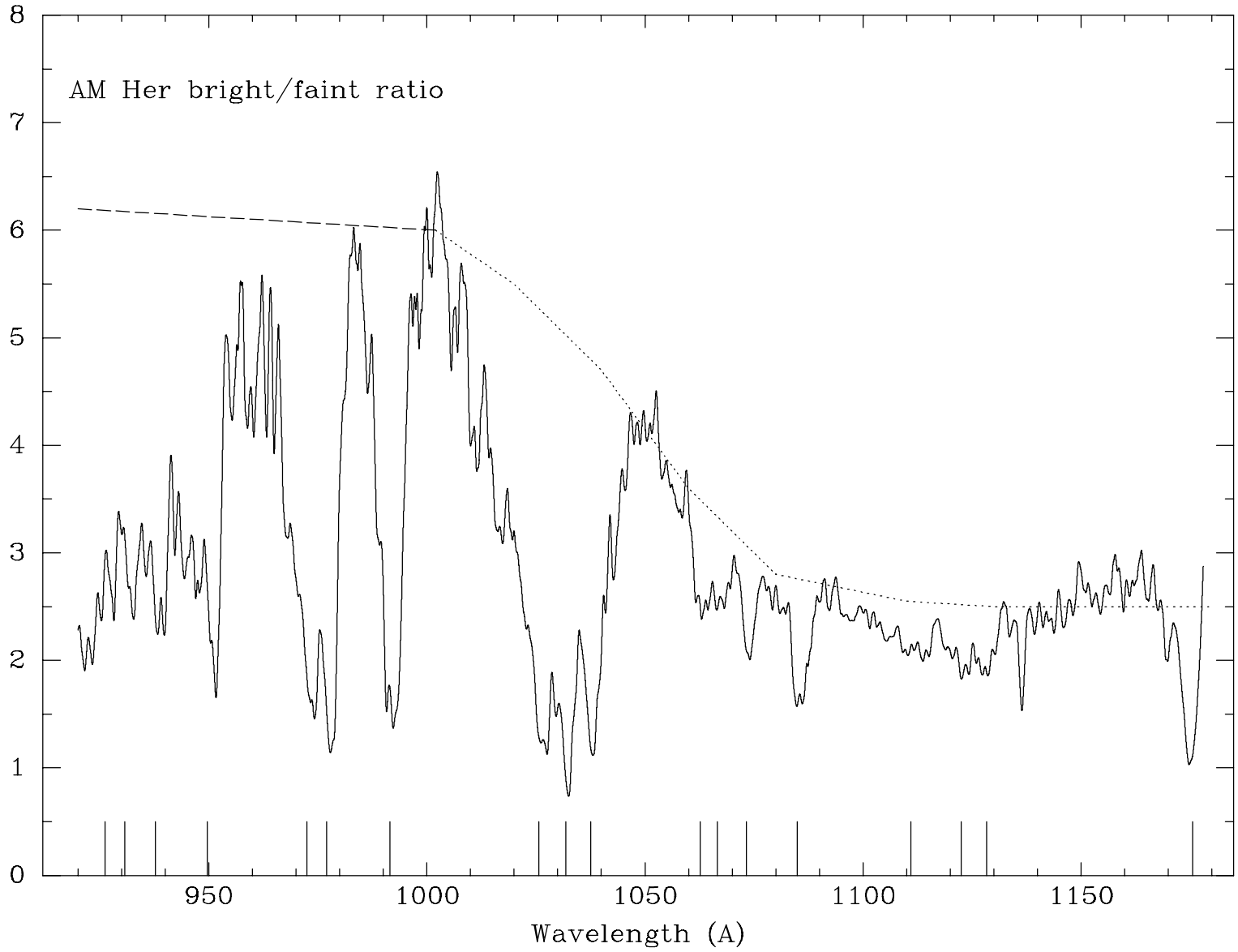
AM Her bright/faint ratio
8
7
6
5
4
3
2
1
0
950
1000
1050
1100
1150
Wavelength (A)

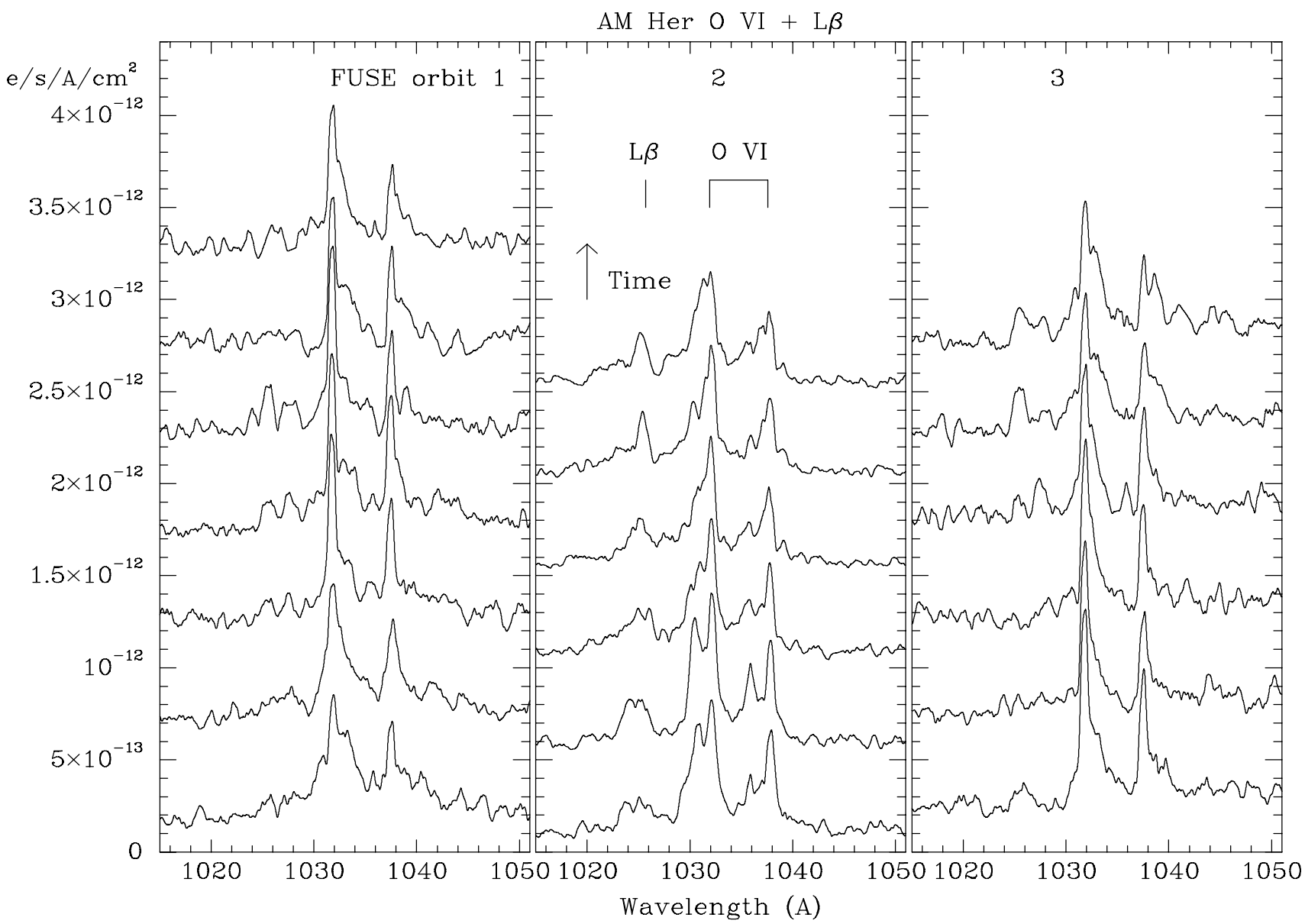
AM Her O VI + Lβ
e/s/A/cm²
FUSE orbit 1
2
3
Lβ
O VI
Time
4×10⁻¹²
3.5×10⁻¹²
3×10⁻¹²
2.5×10⁻¹²
2×10⁻¹²
1.5×10⁻¹²
10⁻¹²
5×10⁻¹³
0
1020
1030
1040
1050
Wavelength (A)

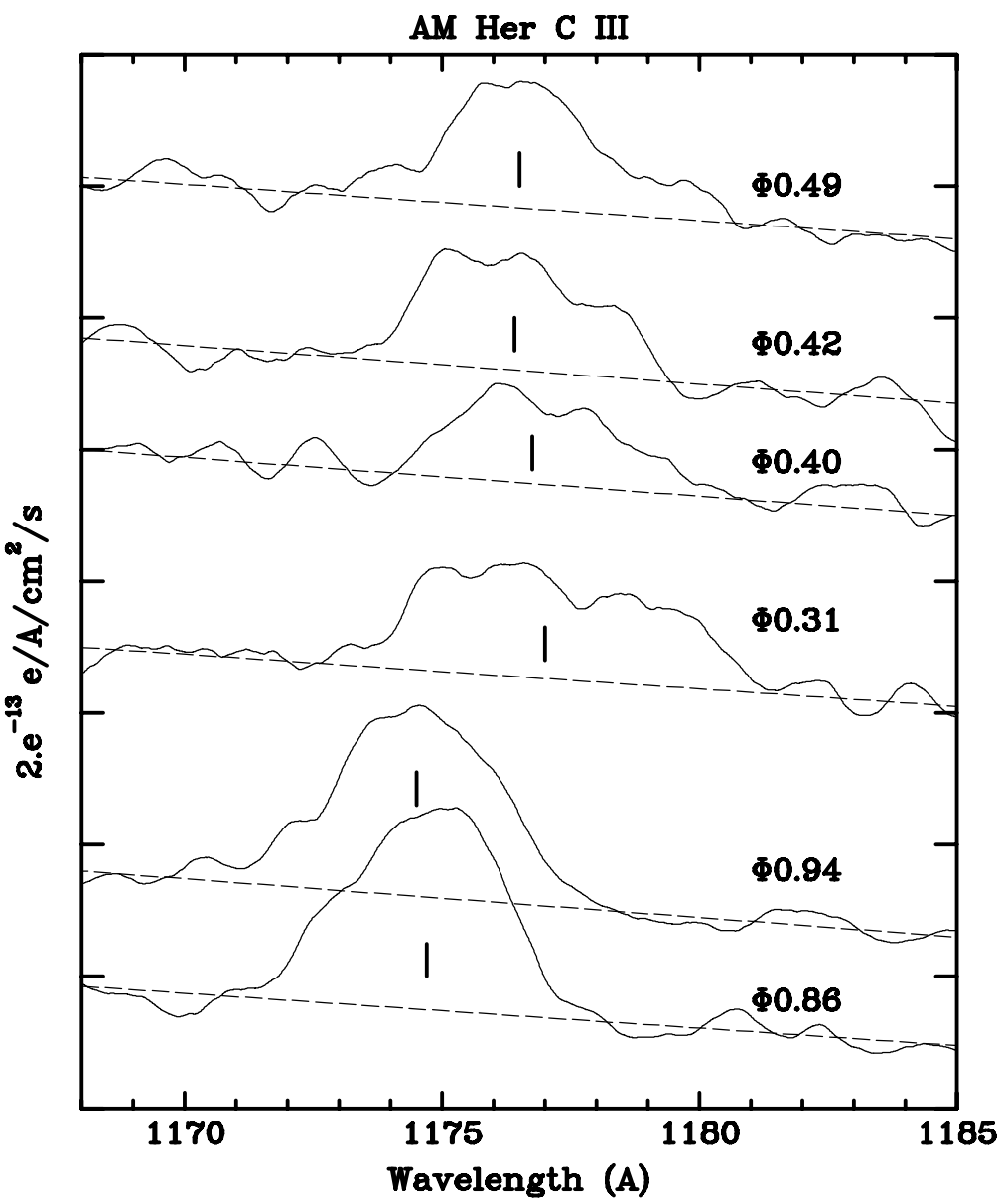
AM Her C III
Φ0.49
Φ0.42
Φ0.40
Φ0.31
Φ0.94
Φ0.86
2.e-13 e/A/cm2/s
1170
1175
1180
1185
Wavelength (A)